Experimental and Theoretical Investigation of the Synthesis, Electronic and Magnetic Properties of MnFe₂O₄ Spinel Ferrite

Khaoula Aghrich [1], Sara Mtougui [2],*, Fayçal Goumrhar [3,4], Mustapha Abdellaoui [2] , Nabila Mamouni [2], Mohammed Fekhaoui [1], Amine El Moutaouakil [5],* and Omar Mounkachi [2,6]

1   Department of Scientific Institute, Mohammed V University in Rabat, Ibn Battouta Avenue,
     Rabat P.O. Box 1014, Morocco
2   Laboratory of Condensed Matter and Interdisciplinary Sciences (LaMCScI), Faculty of Sciences,
     Mohammed V University in Rabat, Ibn Battouta Avenue, Rabat P.O. Box 1014, Morocco
3   Higher School of Education and Training of El Jadida (ESEF), Chouaib Doukkali University,
     El Jadida 24000, Morocco
4   Laboratoire des Sciences de l'Ingénieur pour l'Energie, Ecole Nationale des Sciences Appliquées d'El
     Jadida (ENSA-J), BP 1166, EL Jadida 24002, Morocco
5   Department of Electrical and Communication Engineering, College of Engineering,
     United Arab Emirates University, Al Ain P.O. Box 15551, United Arab Emirates
6   Modeling, Simulation and Data Analysis, Mohammed VI Polytechnic University, Lot 660,
     Hay Moulay Rachid, Ben Guerir 43150, Morocco
*   Correspondence: sara.mtougui@gmail.com (S.M.); a.elmoutaouakil@uaeu.ac.ae (A.E.M.)

Abstract: MnFe₂O₄ ferrite nanoparticle was synthesized via the sol–gel method, and structural, morphology and magnetic characteristics were investigated. X-ray diffraction analysis showed that the synthesized sample was in a single phase with a spinel-ferrite-like structure (space group Fd-3m). The scanning electron microscopy displayed homogenous spherical grains with an agglomeration of the particles. The chemical composition determined by energy-dispersive spectroscopy shows the absence of any impurities. To understand the role of magnetic interaction in MnFe₂O₄ spinel ferrites, the structural and magnetic properties of MnFe₂O₄ have been explored theoretically. Based on the first-principles methods via density functional theory and Monte Carlo simulations, the magnetic hysteresis cycle has been plotted. Using the generalized gradient and GGA-PBE approximation in the full-potential linearized augmented plane wave (FP-LAPW) method, the exchange coupling interactions between magnetic elements and local magnetic moment were evaluated. Furthermore, the theoretical magnetic properties of MnFe₂O₄ were found to match the experimental ones. They both revealed that MnFe₂O₄ is a soft ferromagnetic material. The theoretical curve of magnetization versus temperature indicates that the transition occurred at T_c = 580.0 K. This was also in good agreement with the experimental Curie temperature.

Keywords: magnetic nanoparticle; spinel ferrite; magnetic properties; Monte Carlo simulation

1. Introduction

Nowadays, the study of new materials becomes very interesting and continues to develop rapidly, especially those which can be included in industrial, ecological and technological applications in optoelectronic and piezoelectric fields for instance, where several criteria are to be considered. The field of condensed matter is a very large domain of research. In seeking to satisfy technological needs, several categories of materials have surfaced from three dimensions to zero dimension, such as diluted magnetic semiconductors [1–3], pyrites [4,5], Heusler or half Heusler [6,7], perovskite [8–10] for 3D and phosphorene [11,12], graphene [13–16], MoS₂ [17–19], composite materials [20–23] and silicon-based materials [24] for 2D. Recently, magnetic nanoparticles have been implicated in a wide application domain such as in experimental cancer treatments called magnetic hyperthermia [25], Magnetic immunoassay [26], electrochemical sensing [27], catalyst or

catalyst supports [28,29] and high-density storage [30]. Among the magnetic nanoparticles, there is the class of spinel ferrite oxides (SF) where the main structural formula may be written as MFe_2O_4 (where M = Mn, Fe, Co, Ni, Cu and Zn) [31,32]. Due to their very important characteristics at nanometric sizes, they have emerged as a forwarded category of nanostructured material in the fields of nanoscience and technology. These compounds have soft physical and chemical properties, such as excellent chemical stability, high electromagnetic performance, high cubic magnetocrystalline anisotropy and mechanical hardness [33].

The principal elements that define the magnetic performance of spinel ferrite nanoparticles (NPs) are often acknowledged on several levels: whether on the atomic level, or at the single-particle level as a balance between the magnetically and crystallographically ordered fractions of the NP, as well as at the mesoscopic level by means of mutual interparticle interactions and size distribution phenomena. Generally, the SFs compounds crystallize in a face-centered cubic structure (f.c.c) and belong to the space group Fd3m [34]. The classification of these systems is realized on the basis of the degree of inversion x, and there are three classes, which are based on the spreading of cations at both the tetrahedral (A) and octahedral (B) sites. This degree is the parameter used to distinguish the cation disorder and it is defined as the fraction of M^{2+} ions located in octahedral sites, according to $^T[M_{1-x}Fe_x]^O[M_xFe_{2-x}]O_4$ [35]. As Soufi et al. [36] have reported: when the SF is termed normal spinel, then x = 0; while when it is called an inverse spinel, then x = 1; when 0 < x < 1, it is called mixed spinel. In order to obtain a suitable nanomaterials ferrite, various routes have been used, such as sono-chemical, hydrothermal, sol–gel, co-precipitation and micelle microemulsion [37,38]. These approaches led to different sizes and shapes and hence, to tailoring their properties. It has been signalized that the $MnFe_2O_4$ exhibits a magnetic shift from ferrimagnetic to paramagnetic order around 559.26 K [39]. Using the Monte Carlo simulation, the magnetic characteristics of $CoFe_2O_4$ nanoparticles have been studied [40]. It is found that at room temperature for a size around 21 nm, in the absence of an external magnetic field, the total magnetic moment of the compound is about 1.60 μ_B [40]. On the other hand, while realizing the three-sublattice model it has been displayed that this last one fits well with the super-exchange and the Néel theory of ferrimagnetic material that provide the results of the magnetic properties of ferrites [41]. Bercoff et al. [42] have revealed while studying the compounds Fe_3O_4, $CoFe_2O_4$, $NiFe_2O_4$ and $CuFe_2O_4$ that the condition that allows the validity of the Néels two-sublattice collinear model and the super-exchange theory, is that the interaction between ions in tetrahedral sites should be very weak. Nasri et al. have established the second-order ferromagnetic–paramagnetic (FM-PM) phase transition exhibited by the $CoFe_2O_4$ material at a Curie temperature of 688 K while it decreased when substituting iron by copper [43].

This work reports on the $MnFe_2O_4$ nanoparticles synthesis and structural, morphological and magnetic properties. The obtained nanoparticles by the sol–gel method were analyzed via X-ray diffraction (XRD), scanning electron microscopy (SEM) and the DC extraction method for magnetization measurements. The magnetic properties were explored using DFT and Monte Carlo simulations.

This paper is presented in the following organization: In the experimental section, we present the synthesis process and characterization techniques. After that, we introduce in the simulation section the computational details used in this study. Then, we discuss and compare the synthesis, the calculation magnetization and hysteresis cycles. We finally summarized our results and comparison.

2. Experimental Methods

2.1. Synthesis of MnFe₂O₄ Nanoparticles

Based and inspired by the work of C. Brinker et al. [44], we have modified some experimental conditions for the experiments, such as the nature of precursors and the reaction medium, with the aim of developing a synthesis protocol further to obtain $MnFe_2O_4$ nanoparticles with all the optimized structural and magnetic parameters.

The $MnFe_2O_4$ nanoparticles synthesis was obtained according to the following chemical reaction:

$$MnCl_2 + 2FeCl_3 + 8NaOH \rightarrow MnFe_2O_4 + 4H_2O + 8NaCl$$
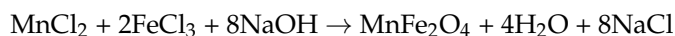
The $MnFe_2O_4$ Nanoparticles were prepared by combining the manganese chloride ($MnCl_2$) (3.7 mmol) and iron chloride III($FeCl_3$) (7.4 mmol), which were liquified separately in 10 mL of purified water and they were mixed in a flask. The obtained solution was kept at 60 °C for 30 min under magnetic stirring. The metal ions were chelated by adding citric acid using the 1:1 ratio. A few drops of a basic solution (NaOH) (11.1 mmol, 10 mL) were used to correct the pH value. The pure solution was treated for 3 h at 80 °C. The mix was positioned in a beaker, then heated softly for several hours at the same temperature until the making of a viscous gel. The gel was also heated overnight at 100 °C to obtain the powder. The obtained sample was grounded and calcined at a temperature of 600 °C for 6 h.

2.2. Characterization Techniques

In this work, the phase, particle size and lattice parameters of the samples were performed by X-ray diffraction (XRD) using a diffractometer with Cu K α radiation (λ = 1.5406 Å). The scanned angular range (2θ) covered from 10° to 70° at a 0.02° step. The applied voltage and current were 45 kV and 100 mA, respectively. The Scanning Electron Microscope (FEI Quanta 450 FEG; Zurich, Switzerland) was utilized to analyze the shape and microstructure of the samples. The magnetic properties were determined using a superconducting quantum interference device (SQUID, Quantum Design, Inc., Darmstadt, Germany).

2.3. Simulation and Computational Analysis

To compare experimental results with theoretical ones, we used both the Density Functional Theory (DFT) calculations and Monte Carlo simulations. Our calculations were based on the full-potential linearized augmented plane wave (FP-LAPW) through the Wien2k package [45]. Based on the Generalized Gradient Approximation with the Coulomb and exchange interaction effects (GGA + U), which is usually used to explore 3d electrons [46], the exchange coupling interactions have been calculated. The self-consistency is achieved by 650 K-points in the irreducible symmetry wedge of the first Brillouin zone. The crystal field of Mn is about 0.51×10^{-3} J/m^3 and for Fe atoms is almost equal to 1.69×10^{-3} J/m^3 and the muffin tin-radii (R_{MT}) of Mn, Fe and O ions are 1.87, 2.13 and 1.5, respectively [39]. We carried out, from our experimental study, the space group and the initial lattice parameter of the $MnFe_2O_4$ compound. It belongs to the Fd-3m space group and the lattice parameter is (a = 8.404 Å).

To study the magnetic behavior of $MnFe_2O_4$ ferrite, Equation (1) shows the Hamiltonian describing this system. As input parameters for Monte Carlo simulation, we used the spin values ($\pm 5/2$) for both Mn^{2+} and Fe^{3+}. These values have been used as input parameters to simulate the magnetic properties, for a predefined system size L = 30 nm, with temperature variation by the Monte Carlo method under the Metropolis algorithm. Resulted data is performed with 10^6 Monte Carlo steps per spin, neglecting the first 10^5 configurations.

$$H = -J_{Mn-Mn} \sum_{\langle i,j \rangle} s_i s_j - J_{Fe-Fe} \sum_{\langle k,l \rangle} \sigma_k \sigma_l - J_{Mn-Fe} \sum_{\langle m,n \rangle} S_m \sigma_n - \Delta_{Mn} \sum_i s_i^2 - \Delta_{Fe} \sum_i \sigma_i^2 - h\left(\sum_i (s_i + \sigma_i)\right) \quad (1)$$

where S and σ are the spins of Mn^{2+} and Fe^{3+}, respectively, J_{Mn-Mn}, J_{Mn-Fe} and J_{Fe-Fe} represent, respectively, the exchange couplings among the first nearest neighbors of Mn-Mn, Mn-Fe and Fe-Fe, Δ_{Mn} and Δ_{Fe} are the octahedral crystal field due to oxygen atoms for Mn and Fe, and h is the external magnetic field.

After the system equilibrium, the following parameters have been calculated for every iteration:

The internal energy:

$$E = \frac{\langle H \rangle}{L^3} \tag{2}$$

The partial magnetizations:

$$M_s = \langle \frac{2}{L^3} \sum_i S_i \rangle \tag{3}$$

$$M_\sigma = \langle \frac{2}{L^3} \sum_i \sigma_i \rangle \tag{4}$$

The total magnetizations:

$$M_T = \frac{M_s + M_\sigma}{2} \tag{5}$$

3. Results and Discussion

3.1. Experimental Results: X-ray Diffraction and SEM Analysis

To determine the average particle size and phase of the synthesized $MnFe_2O_4$ nanoparticles, the X-ray diffraction patterns are depicted in Figure 1. It is clear that the elaborated sample fits well with the spinel ferrite model with a Fd-3 m space group belonging to the reference (JCPDS NO 00-022-1086) and with a lattice constant close to the previously obtained values of bulk $MnFe_2O_4$ [39].
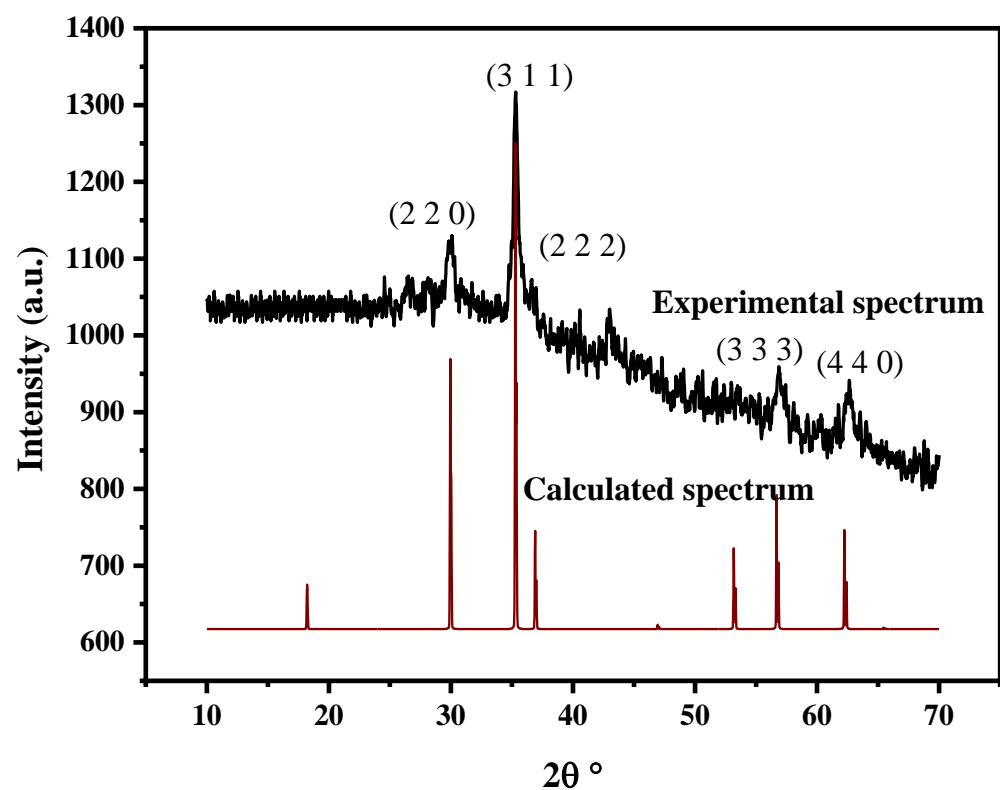

Figure 1. XRD patterns of the synthesized $MnFe_2O_4$.

The strong reflection (hkl) is found to be the (311) plane, which is in good agreement with the same intensified reflection observed in previous works [39,47–49]. The lattice parameters were calculated using the Bragg formula, the cell parameter was estimated to be 8.404 Å, which gives an approximate cell volume of 593.614 $Å^3$.

The Debye-Scherrer formula [50] has been used to calculate the particles size $\langle D \rangle_{XRD}$ from the width of the XRD patterns using the following equation:

$$\langle D \rangle_{XRD} = \frac{K\lambda}{\beta \cos\ \theta} \tag{6}$$

where θ is the Bragg angle, β is the full-width at half-maximum (FWHM) of the reflection peaks, λ is the wavelength of the radiation and the Scherrer constant K is a dimensionless factor with a value close to unity ($\sim$0.9). The lattice parameter, crystallite size values with the same method, sol–gel, and other methods are summarized in Table 1. In this table, the calculations of the crystallite sizes are d_{DRX} = 10.91 nm for the samples calcined in air and d_{DRX} = 20.10–80 nm for the nanoparticles calcined under argon. The lattice parameters by Bragg's law are a = 8.3359 Å and a = 8.2399 Å for nanoparticles calcined in air and under argon, respectively. The lattice parameter of the oxidized sample (calcined in air) corresponds to the value of the lattice parameter of γ-Fe_2O_3 in literature (a = 8.3300 Å), which supports the diffraction pattern indicating the oxidation of the sample. Regarding the sample calcined under argon, the lattice parameter value is different and lower than that of $MnFe_2O_4$ and γ-Fe_2O_3 (also, other cubic elemental lattice oxides such as Fe_3O_4 and Mn_3O_4), which confirms its low crystallinity.

Table 1. XRD patterns of $MnFe_2O_4$ nanoparticles synthetized by several methods.

Samples	Crystallite Size d_{DRX} (nm)	Lattice Parameter a (Å)
Our work	20.00	8.4043
Sample(sol-gel-wheat flour /$MnFe_2O_4$) [51]	16.87	8.4960
Sample (sol-gel-potato flour/$MnFe_2O_4$) [52]	23.12	8.4920
Sample(co-precipitation-calcin in air/$MnFe_2O_4$) [53]	5.0–15.00	8.3359
Sample(co-precipitation-calcin under argon/$MnFe_2O_4$) [54]	20.10–80.00	8.2399

Figure 2 displays SEM pictures and the energy-dispersive X-ray spectroscopy (EDX) spectra, in which the microstructure of the manganese ferrite was investigated, as well as the distribution of its chemical composition. The $MnFe_2O_4$ particles are homogeneous in size and morphology, but they are agglomerated to some degree, which can be justified by the interaction among magnetic nanoparticles. The EDX analysis proves the presence of the Mn, Fe and O elements, which shows the lack of impurities in our obtained compound.
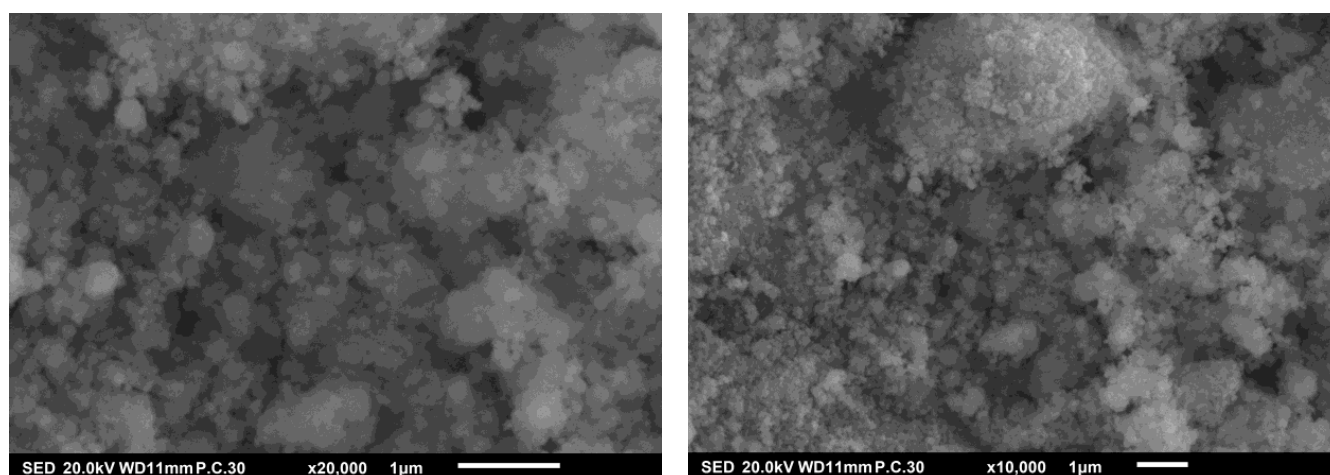

Figure 2. *Cont.*
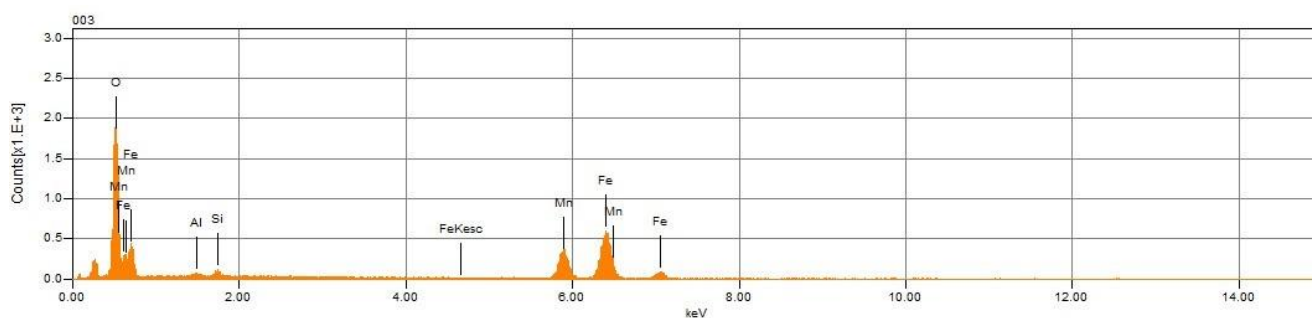
Figure 2. SEM micrographs and EDS spectrum of obtained $MnFe_2O_4$.

To explore the magnetic behavior of the synthesized $MnFe_2O_4$ ferrite nanoparticles, the temperature and the applied magnetic field dependence of magnetization M (H) were also evaluated. The magnetic data of the synthesized $MnFe_2O_4$ ferrite powder were collected for the temperature from 200 K to 800 K, under 500 Oe. The obtained magnetization against temperature M(T) curve is given in Figure 3 at the Curie temperature T_C. This temperature was obtained by the variation of dM(T)/dT as shown in Figure 3. The transition occurred at Tc = 588.0 K, which is in good agreement with the literature [46].
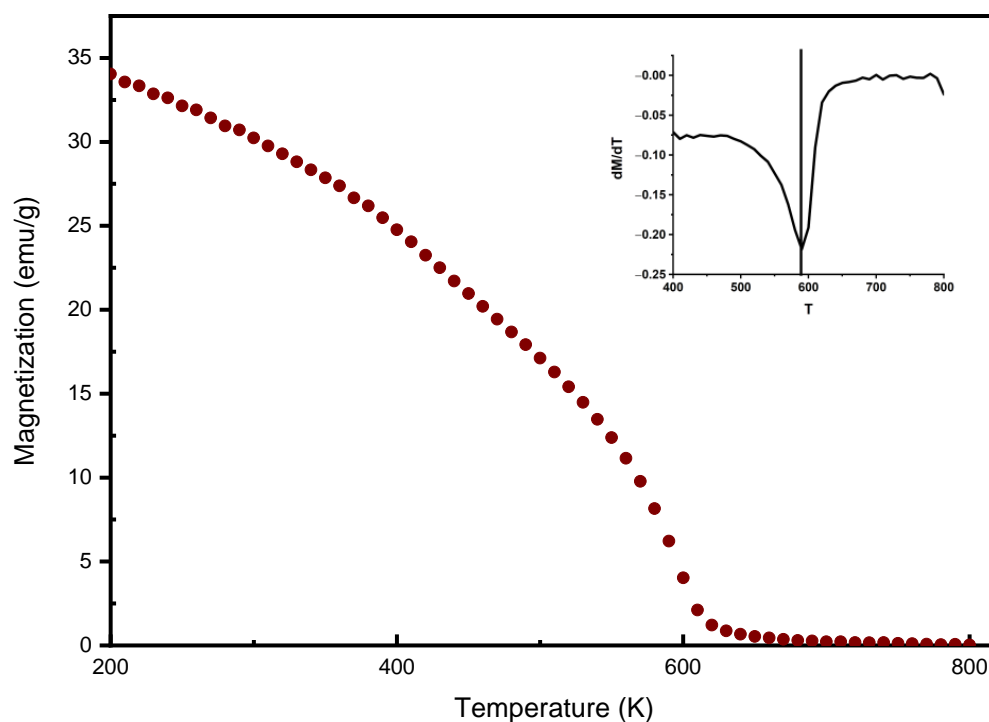

Figure 3. Measured magnetization versus temperature curve for the $MnFe_2O_4$ ferrite. Inset: The temperature dependence of the first derivative of M(T), dM(T)/dT.

The hysteresis cycle for $MnFe_2O_4$ nanoparticles at room temperature T = 300 K is displayed in Figure 4. The magnetization of the $MnFe_2O_4$ nanoparticles was accomplished under a magnetic field from 0 to 60 kOe. From the hysteresis loops, the saturation magnetization (Ms) is about 67.17 emu/g, meaning that this material is heavily magnetic, while the remnant magnetization is Mr = 50 emu/g and the coercive field obtained is about H_C = 113.31 Oe. The magnetization saturation is around M = 67.17 emu/g. The obtained hysteresis behavior of such a ferromagnetic system is interesting for several applications such as anti-lock brake system (ABS) sensor rings [55].
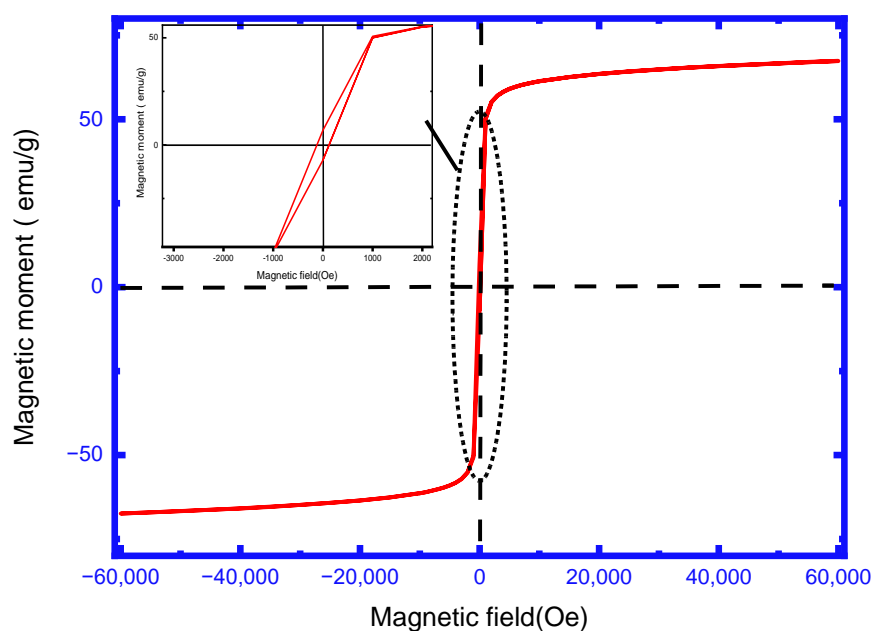
Figure 4. Experimental Hysteresis cycle of MnFe$_2$O$_4$ nanoparticle obtained at 300 K.

3.2. Simulation Results: DFT and Monte Carlo Simulations

We have calculated the magnetic properties and the exchange coupling interactions of the compound MnFe$_2$O$_4$ spinel ferrite with both the GGA and the GGA + U (U = 3 eV) calculations. The ferromagnetic exchange mechanism has been found based on the calculated spin density and magnetic moment. This compound is ferromagnetic with a half-metallic nature [39]. This study obviously explains the important role of the Fe atom in MnFe$_2$O$_4$ [46,49]. Table 2 shows the values of exchange coupling interactions between the first nearest neighbors.

Table 2. Exchange coupling values by GGA + U approximation.

Nearest Neighbors	J$_{Mn-Mn}$	J$_{Mn-Fe}$	J$_{Fe-Fe}$
Exchange couplings (meV)	1.18	−1.87	−1.87

We plot in Figure 5 the calculated magnetization versus temperature curve for the MnFe$_2$O$_4$ ferrite in the absence of an external magnetic field (h = 0). It is found that, for low-temperature values, the magnetization takes its maximum value, i.e., decreasing the temperature causes a decrease in thermal agitation, which leads to rises in magnetization. Furthermore, we notice a second-order phase transition that involves inversions of the Ising system from the ferromagnetic to the paramagnetic phase. This transition is important for a broad spectrum of technological applications [56–58]. Moreover, the obtained curve of magnetization shows a transition from the ferromagnetic to paramagnetic phase at Curie temperature, around Tc = 580.0 K. This is comparable to the experimental Curie temperature displayed in Figure 3. Furthermore, the experimental and theoretical curves exhibit the same pace of magnetization but not the same values of magnetizations. This may be caused by the absence of an external magnetic field in the theoretical part or by a diverse cationic distribution between the two sites A and B of the spinel structure. The calculated magnetization is given in μ$_B$ while the experimental total magnetic moment is in emu/g, and the conversion is drawn from the total magnetic moment to the magnetization using the following formula:

$$M(\text{emu/g}) = \frac{5585}{MW} \times m \ (\mu_B s) \tag{7}$$

where m is the total magnetic moment in μ_B, and MW is the molecular weight of $MnFe_2O_4$ (MW = 230.63 g/mol).
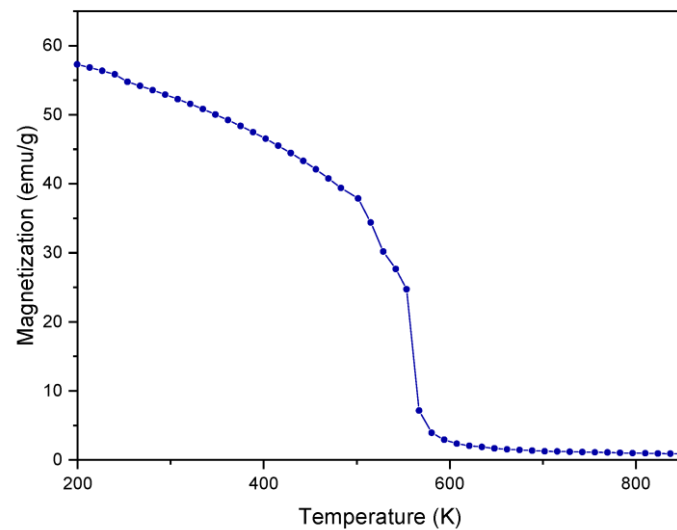

Figure 5. Calculated magnetization versus temperature curve for the $MnFe_2O_4$ ferrite in the absence of external magnetic field.

From the hysteresis loops, we explore the coercive field (H_c), the remanent magnetization (M_r) and the saturation of magnetization (Ms). The obtained coercive field for these nanoparticles is 116.15 Oe at room temperature, which is comparable to the experimental coercive field. The magnetization value at saturation Ms of $MnFe_2O_4$ is 52 emu/g at room temperature, which is in good agreement with the experimental one.

The difference between the saturation magnetization for the experimental and the calculated hysteresis loops is that for the calculated one we consider that the system is perfect which is not the case for the real system. From the hysteresis loops plotted in Figures 4 and 6, $MnFe_2O_4$ is a soft ferromagnetic material, which can be used for transformers, electric machines and/or electromagnets. The cause of the difference in these results is due to the magnetic properties of the nanoparticles that depend on the particle size and the preparation method [56]. This variety is most probably linked also to a different cationic distribution between the two atoms Fe and Mn of the spinel structure.
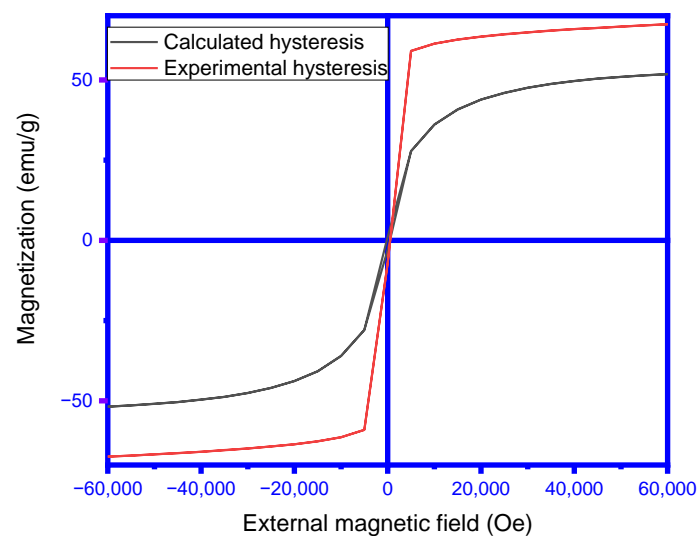

Figure 6. Calculated and experimental Hysteresis cycle of $MnFe_2O_4$ nanoparticle obtained at 300 K.

4. Conclusions

$MnFe_2O_4$ ferrite nanoparticles were obtained via sol–gel method, and the structural, morphology and magnetic characteristics were investigated. The system crystalizes in a single phase with a spinel ferrite-like structure (space group Fd-3m). The structural properties and magnetic properties of $MnFe_2O_4$ have been examined using the first-principles methods via density functional theory and Monte Carlo simulations. The experimental and the calculated Curie temperature of the studied system are obtained at Tc ≈ 588.0 K. From the magnetic hysteresis cycles, $MnFe_2O_4$ is found to be a soft ferromagnetic material, which can be used for transformers, electric machines and/or electromagnets.

Author Contributions: Conceptualization, S.M., A.E.M. and O.M.; Funding acquisition, A.E.M.; Investigation, K.A. and S.M.; Methodology, K.A., S.M., F.G. and M.A.; Supervision, M.F. and O.M.; Validation, M.A., N.M., M.F. and O.M.; Writing—original draft, S.M., A.E.M. and O.M. All authors have read and agreed to the published version of the manuscript.

Conflicts of Interest: The authors declare no competing interests.

References

1. Goumrhar, F.; Bahmad, L.; Mounkachi, O.; Benyoussef, A. Magnetic Properties of Vanadium Doped CdTe: Ab Initio Calculations. *J. Magn. Magn. Mater.* **2017**, *428*, 368–371. [CrossRef]
2. Mediane, N.; Goumrhar, F.; Drissi, L.B.; Laghrissi, M.; Laamara, R.A. High Curie Temperatures and Ferromagnetism Formation in Cr-Substituted Oxide Lithium Compound. *J. Supercond. Nov. Magn.* **2022**, *35*, 463–471. [CrossRef]
3. Mamouni, N.; Goumrhar, F.; Salmani, E.; Benyoussef, A.; Ez-Zahraouy, H.; Mounkachi, O. Spin-Orbit Interaction in SnO_2 Based Diluted Magnetic Semiconductor: Ab-Initio Calculations. *J. Magn. Magn. Mater.* **2021**, *535*, 168084. [CrossRef]
4. Zhao, G.L.; Callaway, J.; Hayashibara, M. Electronic Structures of Iron and Cobalt Pyrites. *Phys. Rev. B* **1993**, *48*, 15781–15786. [CrossRef] [PubMed]
5. Ennaoui, A.; Fiechter, S.; Jaegermann, W.; Tributsch, H. Photoelectrochemistry of Highly Quantum Efficient Single-Crystalline n-FeS_2 (Pyrite). *J. Electrochem. Soc.* **1986**, *133*, 97. [CrossRef]
6. Mouatassime, M.; Selmani, Y.; Idrissi, S.; Bahmad, L.; Goumrhar, F.; Labrim, H.; Benyoussef, A. Magnetic Properties and Half Metallic Behavior of the Full-Heusler Co_2FeGe Alloy: DFT and Monte Carlo Studies. *J. Solid State Chem.* **2021**, *304*, 122534. [CrossRef]
7. Güler, E.; Güler, M.; Uğur, Ş.; Uğur, G. First Principles Study of Electronic, Elastic, Optical and Magnetic Properties of Rh_2MnX (X = Ti, Hf, Sc, Zr, Zn) Heusler Alloys. *Quantum Chem.* **2021**, *121*, e26606. [CrossRef]
8. Bouachraoui, R.; Ziat, Y.; Sbai, Y.; El Rhazouani, O.; Goumrhar, F.; Bahmad, L. The Magnetocaloric and Magnetic Properties of the $MnFe_4Si_3$: Monte Carlo Investigation. *J. Alloy. Compd.* **2019**, *809*, 151785. [CrossRef]
9. Selmani, Y.; Mouatassime, M.; Goumrhar, F.; Labrim, H.; Bahmad, L.; Benyoussef, A. Structural, Electronic and Magnetic Properties of the Perovskite $Ymno_3$. *Solid State Commun.* **2021**, *328*, 114254. [CrossRef]
10. Jonathan, L.; Diguna, L.J.; Samy, O.; Muqoyyanah, M.; Abu Bakar, S.; Birowosuto, M.D.; El Moutaouakil, A. Hybrid Organic–Inorganic Perovskite Halide Materials for Photovoltaics towards Their Commercialization. *Polymers* **2022**, *14*, 1059. [CrossRef]
11. Sahdane, T.; Mtougui, S.; Goumrhar, F.; Mamouni, N.; Salmani, E.; Ez-Zahraouy, H.; Benyoussef, A.; Mounkachi, O. Magnetic Phase Transitions of Phosphorene-like Nano-Structure: Monte Carlo Study. *Philos. Mag.* **2021**, *101*, 1836–1848. [CrossRef]
12. Tiouitchi, G.; Ali, M.A.; Benyoussef, A.; Hamedoun, M.; Lachgar, A.; Kara, A.; Ennaoui, A.; Mahmoud, A.; Boschini, F.; Oughaddou, H.; et al. Efficient Production of Few-Layer Black Phosphorus by Liquid-Phase Exfoliation. *R. Soc. Open Sci.* **2020**, *7*, 201210. [CrossRef]
13. Rao, C.N.R.; Matte, H.S.S.R.; Subrahmanyam, K.S.; Maitra, U. Unusual Magnetic Properties of Graphene and Related Materials. *Chem. Sci.* **2011**, *3*, 45–52. [CrossRef]
14. Panda, J.; Ramu, M.; Karis, O.; Sarkar, T.; Kamalakar, M.V. Ultimate Spin Currents in Commercial Chemical Vapor Deposited Graphene. *ACS Nano* **2020**, *14*, 12771–12780. [CrossRef]
15. Schulz, N.; Chanda, A.; Datt, G.; Kamalakar, M.V.; Sarkar, T.; Phan, M.H.; Srikanth, H. Proximity Enhanced Magnetism at $NiFe_2O_4$/Graphene Interface. *AIP Adv.* **2022**, *12*, 035132. [CrossRef]
16. Moutaouakil, A.E.; Kang, H.-C.; Handa, H.; Fukidome, H.; Suemitsu, T.; Sano, E.; Suemitsu, M.; Otsuji, T. Room Temperature Logic Inverter on Epitaxial Graphene-on-Silicon Device. *Jpn. J. Appl. Phys.* **2011**, *50*, 070113. [CrossRef]
17. Hijazi, A.; Moutaouakil, A.E. Graphene and MoS_2 Structures for THz Applications. In Proceedings of the 2019 44th International Conference on Infrared, Millimeter, and Terahertz Waves (IRMMW-THz), Paris, France, 1–6 September 2019; pp. 1–2.
18. Samy, O.; El Moutaouakil, A. A Review on MoS_2 Energy Applications: Recent Developments and Challenges. *Energies* **2021**, *14*, 4586. [CrossRef]

19. Samy, O.; Zeng, S.; Birowosuto, M.D.; El Moutaouakil, A. A Review on MoS$_2$ Properties, Synthesis, Sensing Applications and Challenges. *Crystals* **2021**, *11*, 355. [CrossRef]

20. Moutaouakil, A.E. Two-Dimensional Electronic Materials for Terahertz Applications: Linking the Physical Properties with Engineering Expertise. In Proceedings of the 2018 6th International Renewable and Sustainable Energy Conference (IRSEC), Rabat, Morocco, 5–8 December 2018; pp. 1–4.

21. El Moutaouakil, A.; Suemitsu, T.; Otsuji, T.; Videlier, H.; Boubanga-Tombet, S.-A.; Coquillat, D.; Knap, W. Device Loading Effect on Nonresonant Detection of Terahertz Radiation in Dual Grating Gate Plasmon-Resonant Structure Using InGaP/InGaAs/GaAs Material Systems. *Phys. Status Solidi (c)* **2011**, *8*, 346–348. [CrossRef]

22. Moutaouakil, A.E.; Suemitsu, T.; Otsuji, T.; Coquillat, D.; Knap, W. Nonresonant Detection of Terahertz Radiation in High-Electron-Mobility Transistor Structure Using InAlAs/InGaAs/InP Material Systems at Room Temperature. *J. Nanosci. Nanotechnol.* **2012**, *12*, 6737–6740. [CrossRef]

23. Moutaouakil, A.E.; Watanabe, T.; Haibo, C.; Komori, T.; Nishimura, T.; Suemitsu, T.; Otsuji, T. Spectral Narrowing of Terahertz Emission from Super-Grating Dual-Gate Plasmon-Resonant High-Electron Mobility Transistors. *J. Phys. Conf. Ser.* **2009**, *193*, 012068. [CrossRef]

24. Meziani, Y.M.; Garcia, E.; Velazquez, E.; Diez, E.; El Moutaouakil, A.; Otsuji, T.; Fobelets, K. Strained Silicon Modulation Field-Effect Transistor as a New Sensor of Terahertz Radiation. *Semicond. Sci. Technol.* **2011**, *26*, 105006. [CrossRef]

25. Rabias, I.; Tsitrouli, D.; Karakosta, E.; Kehagias, T.; Diamantopoulos, G.; Fardis, M.; Stamopoulos, D.; Maris, T.G.; Falaras, P.; Zouridakis, N.; et al. Rapid Magnetic Heating Treatment by Highly Charged Maghemite Nanoparticles on Wistar Rats Exocranial Glioma Tumors at Microliter Volume. *Biomicrofluidics* **2010**, *4*, 024111. [CrossRef] [PubMed]

26. Kwon, O.S.; Lee, S.H.; Park, S.J.; An, J.H.; Song, H.S.; Kim, T.; Oh, J.H.; Bae, J.; Yoon, H.; Park, T.H.; et al. Large-Scale Graphene Micropattern Nano-Biohybrids: High-Performance Transducers for FET-Type Flexible Fluidic HIV Immunoassays. *Adv. Mater.* **2013**, *25*, 4177–4185. [CrossRef] [PubMed]

27. Yang, G.; Zhao, F.; Zeng, B. Magnetic Entrapment for Fast and Sensitive Determination of Metronidazole with a Novel Magnet-Controlled Glassy Carbon Electrode. *Electrochim. Acta* **2014**, *135*, 154–160. [CrossRef]

28. Schätz, A.; Reiser, O.; Stark, W.J. Nanoparticles as Semi-Heterogeneous Catalyst Supports. *Chem. Eur. J.* **2010**, *16*, 8950–8967. [CrossRef]

29. Yoon, T.-J.; Lee, W.; Oh, Y.-S.; Lee, J.-K. Magnetic Nanoparticles as a Catalyst Vehicle for Simple and Easy Recycling. *New J. Chem.* **2003**, *27*, 227–229. [CrossRef]

30. Sun, X.; Huang, Y.; Nikles, D.E. FePt and CoPt Magnetic Nanoparticles Film for Future High Density Data Storage Media. *Int. J. Nanotechnol.* **2004**, *1*, 328–346. [CrossRef]

31. Harris, V.G. Modern Microwave Ferrites. *IEEE Trans. Magn.* **2012**, *48*, 1075–1104. [CrossRef]

32. Datt, G.; Bishwas, M.S.; Raja, M.M.; Abhyankar, A.C. Observation of Magnetic Anomalies in One-Step Solvothermally Synthesized Nickel–Cobalt Ferrite Nanoparticles. *Nanoscale* **2016**, *8*, 5200–5213. [CrossRef]

33. López-Ortega, A.; Lottini, E.; de Julián Fernández, C.; Sangregorio, C. Exploring the Magnetic Properties of Cobalt-Ferrite Nanoparticles for the Development of a Rare-Earth-Free Permanent Magnet. *Chem. Mater.* **2015**, *27*, 4048–4056. [CrossRef]

34. Sivakumar, P.; Ramesh, R.; Ramanand, A.; Ponnusamy, S.; Muthamizhchelvan, C. Synthesis and Characterization of Nickel Ferrite Magnetic Nanoparticles. *Mater. Res. Bull.* **2011**, *46*, 2208–2211. [CrossRef]

35. Granone, L.I.; Ulpe, A.C.; Robben, L.; Klimke, S.; Jahns, M.; Renz, F.; Gesing, T.M.; Bredow, T.; Dillert, R.; Bahnemann, D.W. Effect of the Degree of Inversion on Optical Properties of Spinel ZnFe$_2$O$_4$. *Phys. Chem. Chem. Phys.* **2018**, *20*, 28267–28278. [CrossRef]

36. Soufi, A.; Hajjaoui, H.; Elmoubarki, R.; Abdennouri, M.; Qourzal, S.; Barka, N. Spinel Ferrites Nanoparticles: Synthesis Methods and Application in Heterogeneous Fenton Oxidation of Organic Pollutants—A Review. *Appl. Surf. Sci. Adv.* **2021**, *6*, 100145. [CrossRef]

37. Dippong, T.; Levei, E.A.; Cadar, O. Recent Advances in Synthesis and Applications of MFe$_2$O$_4$ (M = Co, Cu, Mn, Ni, Zn) Nanoparticles. *Nanomaterials* **2021**, *11*, 1560. [CrossRef]

38. Abraime, B.; El Maalam, K.; Fkhar, L.; Mahmoud, A.; Boschini, F.; Ait Tamerd, M.; Benyoussef, A.; Hamedoun, M.; Hlil, E.K.; Ait Ali, M.; et al. Influence of Synthesis Methods with Low Annealing Temperature on the Structural and Magnetic Properties of CoFe$_2$O$_4$ Nanopowders for Permanent Magnet Application. *J. Magn. Magn. Mater.* **2020**, *500*, 166416. [CrossRef]

39. Mounkachi, O.; Lamouri, R.; Salmani, E.; Hamedoun, M.; Benyoussef, A.; Ez-Zahraouy, H. Origin of the Magnetic Properties of MnFe$_2$O$_4$ Spinel Ferrite: Ab Initio and Monte Carlo Simulation. *J. Magn. Magn. Mater.* **2021**, *533*, 168016. [CrossRef]

40. Lamouri, R.; Mounkachi, O.; Salmani, E.; Hamedoun, M.; Benyoussef, A.; Ez-Zahraouy, H. Size Effect on the Magnetic Properties of CoFe$_2$O$_4$ Nanoparticles: A Monte Carlo Study. *Ceram. Int.* **2020**, *46*, 8092–8096. [CrossRef]

41. Srivastava, C.M.; Srinivasan, G.; Nanadikar, N.G. Exchange Constants in Spinel Ferrites. *Phys. Rev. B* **1979**, *19*, 499–508. [CrossRef]

42. Bercoff, P.G.; Bertorello, H.R. Exchange Constants and Transfer Integrals of Spinel Ferrites. *J. Magn. Magn. Mater.* **1997**, *169*, 314–322. [CrossRef]

43. Nasri, M.; Henchiri, C.; Dhahri, R.; Khelifi, J.; Dhahri, E.; Mariano, J.F.M.L. Study of Structural, Magnetic, Magnetocaloric Properties and Critical Behavior of CoFeCuO$_4$ Spinel Ferrite. *Inorg. Chem. Commun.* **2021**, *133*, 108933. [CrossRef]

44. Brinker, C.J.; Scherer, G.W. (Eds.) *Sol-Gel Science*; Academic Press: San Diego, CA, USA, 1990; p. iv. ISBN 978-0-08-057103-4.

45. Schwarz, K. DFT Calculations of Solids with LAPW and WIEN2k. *J. Solid State Chem.* **2003**, *176*, 319–328. [CrossRef]

46. Ong, K.P.; Bai, K.; Blaha, P.; Wu, P. Electronic Structure and Optical Properties of AFeO$_2$ (A = Ag, Cu) within GGA Calculations. *Chem. Mater.* **2007**, *19*, 634–640. [CrossRef]

47. Tang, S.; Zhao, M.; Yuan, D.; Li, X.; Zhang, X.; Wang, Z.; Jiao, T.; Wang, K. MnFe$_2$O$_4$ Nanoparticles Promoted Electrochemical Oxidation Coupling with Persulfate Activation for Tetracycline Degradation. *Sep. Purif. Technol.* **2021**, *255*, 117690. [CrossRef]

48. Baig, M.M.; Zulfiqar, S.; Yousuf, M.A.; Touqeer, M.; Ullah, S.; Agboola, P.; Warsi, M.F.; Shakir, I. Structural and Photocatalytic Properties of New Rare Earth La^{3+} Substituted MnFe$_2$O$_4$ Ferrite Nanoparticles. *Ceram. Int.* **2020**, *46*, 23208–23217. [CrossRef]

49. Sharifi, S.; Rahimi, K.; Yazdani, A. Highly Improved Supercapacitance Properties of MnFe$_2$O$_4$ Nanoparticles by MoS$_2$ Nanosheets. *Sci. Rep.* **2021**, *11*, 8378. [CrossRef] [PubMed]

50. Datt, G.; Raja, M.M.; Abhyankar, A.C. Steering of Magnetic Interactions in Ni$_{0.5}$Zn$_{0.5}$Fe$_2$–x(Mn)$_X$O$_4$ Nanoferrites via Substitution-Induced Cationic Redistribution. *J. Phys. Chem. C* **2021**, *125*, 10693–10707. [CrossRef]

51. Mary Jacintha, A.; Umapathy, V.; Neeraja, P.; Rex Jeya Rajkumar, S. Synthesis and Comparative Studies of MnFe$_2$O$_4$ Nanoparticles with Different Natural Polymers by Sol–Gel Method: Structural, Morphological, Optical, Magnetic, Catalytic and Biological Activities. *J. Nanostruct. Chem.* **2017**, *7*, 375–387. [CrossRef]

52. Chen, J.P.; Sorensen, C.M.; Klabunde, K.J.; Hadjipanayis, G.C.; Devlin, E.; Kostikas, A. Size-Dependent Magnetic Properties of MnFe$_2$O$_4$ Fine Particles Synthesized by Coprecipitation. *Phys. Rev. B* **1996**, *54*, 9288–9296. [CrossRef] [PubMed]

53. Ostler, T.A.; Barker, J.; Evans, R.F.L.; Chantrell, R.W.; Atxitia, U.; Chubykalo-Fesenko, O.; El Moussaoui, S.; Le Guyader, L.; Mengotti, E.; Heyderman, L.J.; et al. Ultrafast Heating as a Sufficient Stimulus for Magnetization Reversal in a Ferrimagnet. *Nat. Commun.* **2012**, *3*, 666. [CrossRef]

54. Amighian, J.; Mozaffari, M.; Nasr, B. Preparation of Nano-Sized Manganese Ferrite (MnFe$_2$O$_4$) via Coprecipitation Method. *Phys. Status solidi (c)* **2006**, *3*, 3188–3192. [CrossRef]

55. Bas, J.A.; Calero, J.A.; Dougan, M.J. Sintered Soft Magnetic Materials. Properties and Applications. *J. Magn. Magn. Mater.* **2003**, *254–255*, 391–398. [CrossRef]

56. Aghrich, K.; Abdellaoui, M.; Mamouni, N.; Bellaouchou, A.; Fekhaoui, M.; Hlil, E.K.; Mounkachi, O. Experimental and First-Principles Study of the Origin of the Magnetic Properties of CoFe$_2$O$_4$ Spinel Ferrite. *Appl. Phys. A* **2020**, *126*, 940. [CrossRef]

57. Kumar, V.; Rana, A.; Yadav, M.S.; Pant, R.P. Size-Induced Effect on Nano-Crystalline CoFe$_2$O$_4$. *J. Magn. Magn. Mater.* **2008**, *320*, 1729–1734. [CrossRef]

58. Biswas, A.; Zarkevich, N.A.; Pathak, A.K.; Dolotko, O.; Hlova, I.Z.; Smirnov, A.V.; Mudryk, Y.; Johnson, D.D.; Pecharsky, V.K. First-Order Magnetic Phase Transition in Pr$_2$In with Negligible Thermomagnetic Hysteresis. *Phys. Rev. B* **2020**, *101*, 224402. [CrossRef]